drones

MDPI

Article

Canopy Structural Changes in Black Pine Trees Affected by Pine Processionary Moth Using Drone-Derived Data

Darío Domingo [1,2], Cristina Gómez [1,3], Francisco Mauro [1], Hermine Houdas [1], Gabriel Sangüesa-Barreda [1] and Francisco Rodríguez-Puerta [1,*]

[1] iuFOR, EiFAB, University of Valladolid, 42004 Soria, Spain; dario.domingo@uva.es (D.D.); cgomez@uva.es (C.G.); francisco.mauro@uva.es (F.M.); herminejosephine.houdas@uva.es (H.H.); gabriel.sanguesa@uva.es (G.S.-B.)
[2] GEOFOREST-IUCA, Department of Geography, University of Zaragoza, Pedro Cerbuna 12, 50009 Zaragoza, Spain
[3] Department of Geography and Environment, School of Geoscience, University of Aberdeen, Aberdeen AB24 3UE, Scotland, UK
* Correspondence: francisco.rodriguez.puerta@uva.es

Abstract: Pine species are a key social and economic component in Mediterranean ecosystems, where insect defoliations can have far-reaching consequences. This study aims to quantify the impact of pine processionary moth (PPM) on canopy structures, examining its evolution over time at the individual tree level using high-density drone LiDAR-derived point clouds. Focusing on 33 individuals of black pine (*Pinus nigra)*—a species highly susceptible to PPM defoliation in the Mediterranean environment—bitemporal LiDAR scans were conducted to capture the onset and end of the major PPM feeding period in winter. Canopy crown delineation performed manually was compared with LiDAR-based methods. Canopy metrics from point clouds were computed for trees exhibiting contrasting levels of defoliation. The structural differences between non-defoliated and defoliated trees were assessed by employing parametric statistical comparisons, including analysis of variance along with post hoc tests. Our analysis aimed to distinguish structural changes resulting from PPM defoliation during the winter feeding period. Outcomes revealed substantive alterations in canopy cover, with an average reduction of 22.92% in the leaf area index for defoliated trees, accompanied by a significant increase in the number of returns in lower tree crown branches. Evident variations in canopy density were observed throughout the feeding period, enabling the identification of two to three change classes using LiDAR-derived canopy density metrics. Manual and LiDAR-based crown delineations exhibited minimal differences in computed canopy LiDAR metrics, showcasing the potential of LiDAR delineations for broader applications. PPM infestations induced noteworthy modifications in canopy morphology, affecting key structural parameters. Drone LiDAR data emerged as a comprehensive tool for quantifying these transformations. This study underscores the significance of remote sensing approaches in monitoring insect disturbances and their impacts on forest ecosystems.

Keywords: canopy structure; drone-based remote sensing; forest ecosystem monitoring; insect disturbances; pine processionary moth

Citation: Domingo, D.; Gómez, C.; Mauro, F.; Houdas, H.; Sangüesa-Barreda, G.; Rodríguez-Puerta, F. Canopy Structural Changes in Black Pine Trees Affected by Pine Processionary Moth Using Drone-Derived Data. *Drones* **2024**, *8*, 75. https://doi.org/10.3390/drones8030075

Academic Editor: Tim Whiteside

Received: 11 January 2024
Revised: 16 February 2024
Accepted: 20 February 2024
Published: 22 February 2024

1. Introduction

Herbivorous insects are natural catalysts for disturbance within forest ecosystems. However, the increasing frequency and heightened virulence of outbreaks, attributed to climate warming, have raised significant concerns in forest management [1,2]. Insect outbreaks have impacts on forest resilience and crucial forest ecosystem services, including carbon sequestration and timber production [3,4]. The effects of outbreaks on host trees span a spectrum, ranging from growth decline to eventual mortality. Moreover, they often interact with other pathogens and drought stress, leading to non-lineal responses

and excessive mortality [5]. In the Mediterranean region, one of the major defoliating insects affecting pines and cedars is the pine processionary moth (PPM, *Thaumetopoea pityocampa*) [6]. PPM defoliations are widespread in Spanish forests, annually affecting 500,000 ha [7], reducing tree growth and subsequently its carbon storage capacity [4].

The life cycle of PPM commences in summer when adult female moths, which have a brief lifespan of approximately one night, lay up to 300 eggs on pine needles after mating [8]. These eggs then hatch into larvae, which proceed to feed on pine needles throughout the winter. Once the fifth and last instar of the larval development stage starts concluding, the larvae organize into processions and move from the canopy to the ground, undergo pupation in the soil, and eventually give rise to new adult moths in the following summer. Alternatively, some may enter a short or prolonged diapause [9]. PPM has the potential to instigate large-scale outbreaks characterized by intense defoliation, although it rarely causes tree mortality, underscoring the high resilience of tree host species to this endemic pest. Nevertheless, it does curtail tree growth and reproductive capacity [4,10]. Additionally, the caterpillar hairs can induce severe allergic reactions for humans and animals, resulting in skin lesions or respiratory difficulties, posing a threat to public health [11]. The population size of PPM is significantly influenced by environmental conditions, such as climatic factors, interactions with other species, and the composition and structure of the forests [12,13]. The performance of PPM is strongly constrained by temperature, with lethal thresholds for PPM larvae ranging from −12 to −16 °C in winter [14,15] and for PPM eggs between 36 and 42 °C in summer [16,17]. Warmer winters are expanding PPM outbreaks northward and to higher elevations [15], while adverse effects have also been observed due to the increasing severity of heat events [18–20]. Precipitation levels influence the lignin content of pine needles, leading, in cases of water stress, to lower nutritional properties that adversely affect PPM populations [10,21]. Furthermore, there is consensus on the high vulnerability of *Pinus nigra* [22] over other species within the same genus. Forest composition, generally measured by species richness, reduces PPM abundance particularly when non-host tree species are present [23–25]. PPM performance also depends on forest structure, increasing its incidence in structurally simple pine forests such as monospecific plantations [13]. Less consensus has been found on the effects of forest age [12]. Tree location at the landscape scale matters, causing forest edges and isolated trees to be more vulnerable to PPM defoliation [26]. Consequently, given the anticipated rise in temperatures and the frequency of extreme events, which may result in unpredictable PPM development, it is paramount to develop cost-effective tools for monitoring the spatiotemporal effects on conifer forests that serve as base information for forest composition and structure management.

Practically, the monitoring of PPM traditionally relies on visual assessments by forestry technicians or photo interpreters gauging the degree of infestation in the field [8]. In Spain, for instance, about 70% of regions employ PPM monitoring programs, predominantly based on in situ surveys. These programs are supplemented by additional assessments on specific plots by the International Co-operative Programme on Assessment and Monitoring of Air Pollution Effects on Forests (ICP Forest). While in situ surveys are valuable, their associated costs, resource demands and, at times, temporal intervals may constrain effective forest management actions. The integration of remote sensing, leveraging the rapid advancements in platforms and sensors, provides quantitative insights that not only complements in situ surveys but also enhances the spatiotemporal frequency of observations.

Remote sensing has gained significant attention for analyzing insect disturbances and monitoring their dynamics across three key species groups: bark beetles and broadleaved and coniferous defoliators [27]. Notably, time series data acquired by the Moderate Resolution Imaging Spectroradiometer (MODIS) have been employed to monitor PPM defoliations in homogeneous managed stands of *Pinus pinaster* at southwest France [28] with correlations up to 0.9 when using the enhanced vegetation index. Likewise, Landsat data have been utilized to significantly differentiate up to three defoliation levels in northeastern [29] and southeastern [30] Spain, with the moisture stress index (MSI), normalized difference infrared index (NDII), and normalized burn ratio (NBR) being the most suitable spectral

indices for this purpose. The increased availability of drone derived data has introduced novel spatial scales for analyzing PPM defoliation at the individual tree level. RGB orthomosaics showed a 79% accuracy in discriminating between defoliated and non-defoliated trees in two study sites dominated by *Pinus sylvestris*, *Pinus halepensis*, and *Pinus nigra* at northeast Spain (Solsona) [8]. Multispectral drone information was used to determine three defoliation classes with 82% accuracy in a mixed forest dominated by *Quercus ilex* and *Pinus sylvestris* at northeast Spain (Solsona) [31,32]. Additionally, Otsu et al. [33] calibrated Landsat 8 with drone multispectral imagery to detect PPM defoliations. While much of the literature concentrates on PPM detection and the quantification of its infestation levels, García et al. [34] explored the use of drone-derived RGB data in conjunction with artificial intelligence models to detect PPM nests. Despite previous studies having predominantly focused on the analysis of PPM defoliations and their effects based on two-dimensional data, there has been limited attention given to the three-dimensional changes in forest cover due to PPM disturbances. This is crucial to better understand the links between coverage change and tree growth reduction. This scarcity may be attributed to the lack of high-density 3D multitemporal flights, such as those derived from LiDAR sensors carried out by drones. This information presents innovative perspectives for addressing questions such as what are the effects of insect defoliation on crown morphology and forest structure? What are the volume changes (e.g., crown volume) caused by an insect outbreak? These inquiries contribute to the monitoring of forest ecosystems, providing pertinent information for effective forest management actions.

In this study, our primary objective is to assess the efficacy of high-density drone LiDAR-derived point clouds in quantifying the impact of PPM on canopy structure and its development over time at individual tree level scale. In particular, this study attempts to (i) investigate the existence of structural differences between non-defoliated and PPM-defoliated trees, (ii) evaluate the potential of drone-derived LiDAR data to discern structural changes attributable to PPM defoliation over time (i.e., along a feeding winter period), and (iii) analyze the disparities between manual tree crown detection and automatized LiDAR-derived crowns concerning structural metrics associated with PPM defoliations. To achieve these objectives, our focus is on a black pine (*Pinus nigra* subsp. *salzmannii)* forest, as it represents a highly susceptible species to PPM defoliations in the Mediterranean environment.

2. Materials and Methods

2.1. Study Area and Field Data Collection

This study was conducted at the Cañón del Rio Lobos Natural Park (10,202 ha), located in the western region of Soria province (Figure 1). The selected area comprises a forest stand dominated by *Pinus nigra* subsp. *salzmannii*, a pine species highly vulnerable to PPM attacks [13]. The stand is complemented by *Juniperus thurifera* trees and shrub strata dominated by *Cistus laurifolius* and *Juniperus communis*. The topography of the stand is generally flat, with elevations ranging from 1138 to 1168 m above sea level. The mean annual temperature in this region is 9.2 °C, and the annual rainfall reaches 670 mm. The predominant lithology consists of upper Cretaceous conglomerates and loams.

Field data were gathered from 33 trees through visual assessment conducted at the individual tree level. This assessment was carried out by two experts simultaneously employing binoculars for enhanced precision. Each pine tree was assigned a defoliation value, expressed as a percentage ranging from 0%, indicating no defoliation, to 100%, signifying complete defoliation, in 5% intervals. Field campaigns were executed in close proximity to the acquisition flight dates, specifically during the third week of December 2022 and the first week of May 2023 (Figure 2). This timing ensured that there were no alterations in defoliation levels, aligning roughly with the commencement and conclusion of the major feeding period in winter.

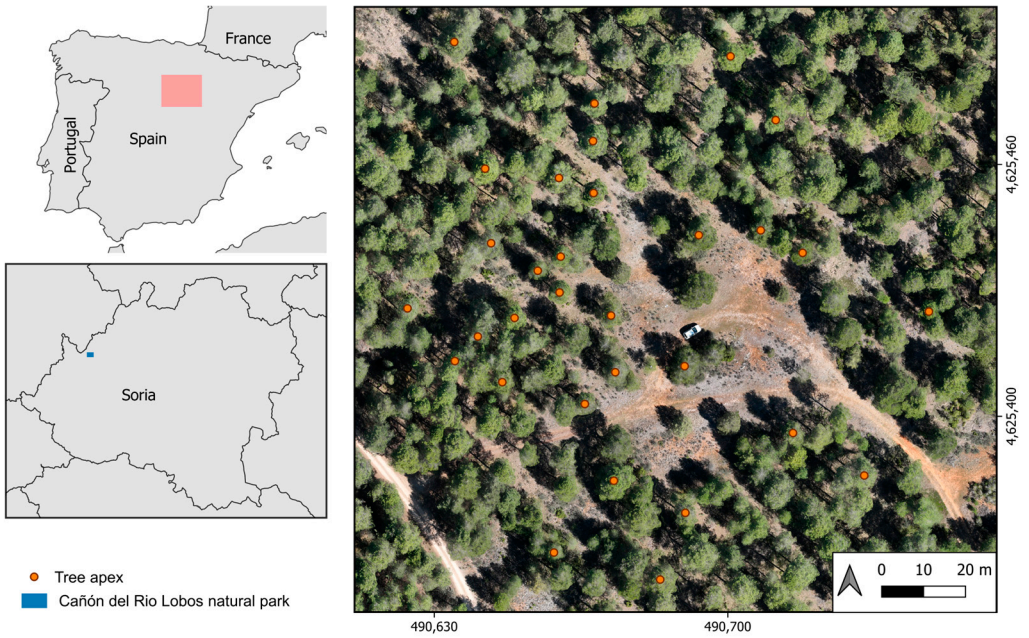

Figure 1. Study area location and distribution of the 33 field inventoried trees. The orthomosaic was derived from a drone DJI Mavic 3 RTK flight with an RGB camera carried out in April 2023.

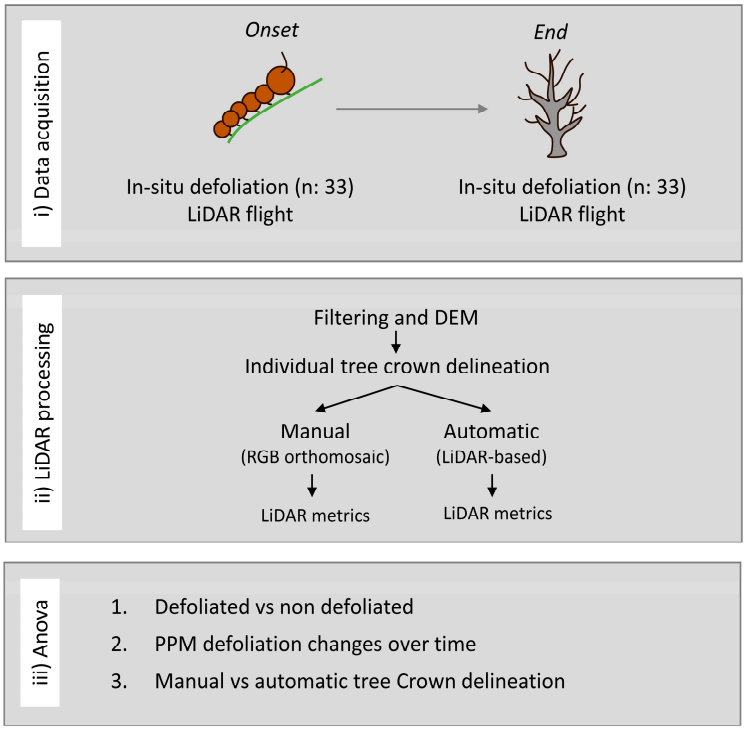

Figure 2. Methodological flowchart.

Table 1 shows a summary of the defoliation attributes obtained from the 33 field measured trees. The defoliation values increased, on average, to 10.43% along the analyzed feeding period, while the increase in nests was lower, with an average change in roughly two nests. Nine trees showed defoliation levels below 15% in both of our field campaigns, being designated as non-defoliated.

Table 1. Average observed tree defoliation (n = 33), values in parenthesis represent the observed range (minimum–maximum).

Field Campaign	% Defoliation	Number of Nests
First (December 2022)	10.00 (0–35)	5.8 (0–21)
Second (May 2023)	20.43 (0–45)	7.5 (0–21)

2.2. Drone LiDAR Data Acquisition and Preprocessing

The drone LiDAR point clouds were acquired through two flights conducted in the first week of January 2023 and the fourth week of March 2023, capturing the onset and conclusion of the PPM feeding period. The data collection utilized a DJI Matrice 300 RTK drone equipped with a DJI Zenmuse L1 LiDAR sensor (Table 2). The L1, a discrete return sensor operating at a wavelength of 905 nm has dimensions of 152 × 110 × 169 mm and weights of 0.930 kg. It incorporates an inertial measurement unit (IMU) for precise control of flight parameters. The sensor employed an average pulse repetition frequency of 160 KHz, capturing up to three returns per pulse, with an average RMSE in z values of 0.05 m. The Matrice 300, weighing 6.3 kg without payload, was equipped with a global navigation satellite system (GNSS) and real-time kinematic (RTK) capabilities to ensure accurate positioning during flight operations. Point cloud acquisition was planned prior to flight and managed in real time using the Pilot 2 software version 7.1 installed in the DJI Matrice 300 controller. The flight altitude above ground was set to 50 m, providing a nominal point density of at least 500 points m^{-2} for both acquisitions.

Table 2. Summary of the LiDAR flight characteristics for each acquisition.

Acquisition Parameters	Onset PPM Feeding Period	Conclusion PPM Feeding Period
Date (day-month-year)	10 January 2023	24 April 2023
Flight height	50	50
Side Overlap (%)	80	80
Point density	2021.49 points × m^{-2}	1120.05 points × m^{-2}
Pulse density	1603.78 pulses × m^{-2}	870.76 pulses × m^{-2}
Area (ha)	10.43	13.35
Data size (GB)	2.13	1.41

The preprocessing of drone LiDAR point clouds was conducted using DJI Terra proprietary software version 3.6.6. All acquired returns were retained within an effective distance from point cloud up to 250 m. The resulting point clouds were generated in the WGS 84 Universal Transverse Mercator (UTM) zone 30 N (EPSG:32630) incorporating EGM2008 height geoid correction. To enhance data quality, noise was filtered, and duplicates were removed from the point clouds. Subsequently, the point clouds were classified into ground and non-ground (vegetation) categories using a refined version of the triangulated irregular network (TIN) from Axelsson [35] implemented in LAStools [36]. A digital elevation model (DEM) with a 0.10 m grid resolution was then generated using the weighted linear least squares interpolation-based method [37].

2.3. Individual Tree Crown Delineation

The delineation of tree crown was executed employing two distinct methodologies: manual delineation and LiDAR-based delineation.

In the manual delineation approach, the initial step involved recording the coordinates of individual trees through a sub-metric GPS receiver (Trimble Geo 7X, Trimble Geospatial, Dubai, United Arab Emirates). Subsequently, a simultaneous RGB orthomosaic was captured on 24 April 2023 utilizing a Mavic 3 Multispectral (M3M) drone (see Table A1 Appendix A for flight acquisition parameters) that integrates a RTK module ensuring centimetric x, y, and z positions. The orthomosaic was employed to manually digitalize the crowns for the selected 33 trees. The manual delineation did not entail the

use of LiDAR point cloud. This process was accomplished using QGIS software version 3.30.3 (QGIS Development Team, 2023).

The LiDAR-based delineation automatizes the identification of treetops and crown boundaries. Our individual tree detection (ITD) process utilized the ForestTools package in R [38]. This methodology involved a double-loop algorithm that iteratively adjusted two critical parameters, namely intercept (ranging from 0.5 to 1.0 in 0.1 increments) and slope (ranging from 0 to 0.4 in 0.05 increments) of the vwf [39] and mcws [40] functions, respectively. These parameters significantly influence the variable window filter and marker-controlled watershed segmentation, essential for treetop detection and subsequent crown delineation. Systematically varying intercept and slope allowed us to generate a series of potential tree and crown delineations. Each iteration produced vector files representing treetops and crown polygons, which were then visually inspected against RGB imagery derived from drone data to identify the most accurate representation of the forest canopy (Figure A3 Appendix A). This visual assessment facilitated an empirical determination of the optimal parameter settings, ensuring the highest fidelity in representing individual trees and their crowns. Subsequently, we employed the QGIS delete holes function with a surface up to 5 cm^2 to ensure that no voids were present within the LiDAR-delimited crowns.

The manual and LiDAR-based crown delineations, once selected, formed the basis for an extensive metric analysis. This analysis delved into various canopy characteristics, shedding light on the extent of PPM caterpillar infestation.

2.4. LiDAR Metric Computation for Individual Trees

The computation of LiDAR metrics involved the analysis of four datasets, encompassing two crown delineations (manual and LiDAR-based) and two flights (pre and post feeding period). Point clouds were clipped to match the spatial extent of individual tree crowns. Return heights were normalized by subtracting the DEM created at 0.10 m (see Section 2.2). Subsequently, a full suite of statistical metrics commonly used for forestry purposes was derived [41–43]. Statistics pertaining to height distribution (CHM) and variability (CHVM), canopy density (CHD), structural diversity indices (SDI) [44,45], and metrics based on the voxelizing point cloud [43] were computed (see Table A2 Appendix A for a detailed list of computed metrics). A threshold value of 2 m height was applied to remove ground and understory laser hits before generating the ALS-derived variables according to Nilsson [46] and Næsset and Økland [47]. The metric computation was performed using lidR package [48–50], lidRmetrics [43], lasR [42], and FUSION [37].

Canopy structural differences between the flights were determined by subtracting the post PPM feeding period flight (April) from the onset of the major feeding period flight (January). This approach enabled us to characterize the changes attributable to PPM infestation for subsequent analysis (see Section 2.5).

2.5. Analysis of Morphological Differences at Tree Level Scale

The analysis of morphological differences was conducted on a threefold basis in alignment with our objectives. To investigate whether structural disparities existed between trees with differences in defoliation, we categorized the trees into two classes. Following the approach by Cardil et al. [31], pines with defoliation levels below 15%, as measured in both of our field campaigns, were designated as non-defoliated (n: 11 trees), while those with higher values were classified as defoliated (n: 22 trees). We conducted the Shapiro–Wilk test to check that the population had a normal distribution and the Breusch–Pagan homogeneity test to ensure that classes had similar variance. Logarithmic and square root transformations were explored in cases where statistical hypothesis could not be fulfilled. Subsequently, an analysis of variance (ANOVA) test was employed to determine whether significant statistical differences existed in their structural properties between non-defoliated and defoliated trees.

Our second objective aimed to assess the potential of drone-derived LiDAR data in discerning structural changes resulting from PPM defoliation over time. Initially, we established two classes, distinguishing between no change (n: 23 trees) and change in defoliation (n: 10 trees). The breakpoint between these classes was set at a 10% change, a commonly used threshold in field observations. Additionally, we introduced three classes (no change, small change, and great change in defoliation) using a k-means clustering analysis. K-means is a classic method known for its adaptability to new datasets, simplicity in implementation, and scalability to large datasets. The breakpoints defined by K-means algorithm was set at 5%, 15%, and >15% change for no change (n: 12 trees), small change (n: 13 trees), and great change (n: 6 trees) in defoliation classes, respectively. Consistent with the previous analysis (Aim 1), we conducted normality and homogeneity tests, followed by an ANOVA test, to investigate whether LiDAR-derived structural metrics could effectively detect changes in PPM defoliation.

Finally, to examine the dissimilarity between manual tree crown detection and automatized LiDAR-based crown delineation concerning derived structural metrics, we employed an ANOVA test. Subsequent to this, a Tukey post hoc test was applied to metrics that exhibited significant differences in earlier analyses (Aims 1 and 2).

3. Results

3.1. Structural Differences between Non-Defoliated and Defoliated Trees

The impact of PPM infestation is reflected in reduced tree crown density as observed in the canopy cover LiDAR-derived metrics derived for both manually and automatically delineated. For both crown delineation methods, statistically significant differences, with 95% of probability, were identified for five LiDAR-derived metrics (Table 3). Notably, a direct correlation was observed between the degree of defoliation and the decline in values for leaf area index proxy and mean leaf area density proxy (hereinafter leaf area index and mean leaf area density), experiencing a significant average reduction of up to 22.92% and 22.88%, respectively (Figure 3, Figure A1 of Appendix A). The diminished presence of crown needles resulting from PPM feeding leads to increased LiDAR pulse penetration and a higher number of returns in lower tree crown branches. Consequently, statistically significant differences were noted in three LiDAR-derived metrics associated with the presence of lower tree crown branches or higher penetration of first returns. For example, there was an average increase of 7.45% in the ratio between the number of returns above 2 m and total number of first returns in defoliated trees. Additionally, the percentage of returns in the lower 10% or 20% of the maximum elevation increased by 1.33% and 3.10%, respectively, in non-healthy trees.

Table 3. Summary of the LiDAR metrics with statistically significant differences between defoliated and non-defoliated trees for manual and LiDAR based crown delineation. Values in parenthesis indicate the absolute differences between non-defoliated and defoliated trees.

LiDAR Metric	Manual Delimitation ANOVA (*p* Value)	LiDAR Based Crown ANOVA (*p* Value)	Transformation
Leaf area index	0.02 (2.71)	0.03 (2.44)	None
Mean leaf area density	0.02 (0.24)	0.03 (0.22)	None
% all returns above 2 m respect to total first returns	0.02 (7.46)	0.01 (8.22)	None
% returns in lower 10% of maximum elevation (W1)	0.03 (1.33)	0.04 (1.24)	Logarithmic
% returns in lower 20% of maximum elevation (W2)	0.02 (3.11)	0.04 (3.29)	Logarithmic

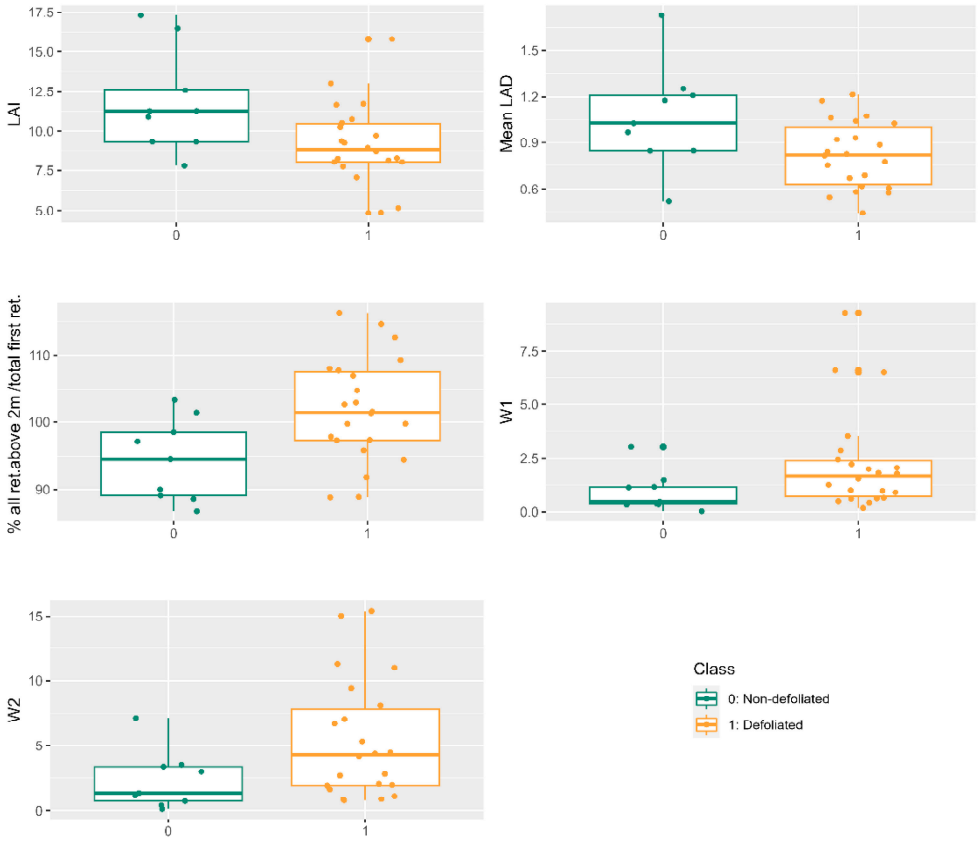

Figure 3. Boxplots of LiDAR metrics for non-defoliated vs. defoliated trees (class 0 vs. class 1) for manual crown delineation. LAI refers to leaf area index; Mean LAD stands for mean leaf area density; % all ret. above 2 m/total first ret. refers to the percentage of all returns above 2 m respect to total first returns; W1 and W2 are the % returns in lower 10 or 20% of maximum elevation, respectively.

3.2. Structural Changes over the PPM Feeding Period

PPM induces notable modifications in canopy structure during the major feeding period in winter. Canopy LiDAR-derived metrics reveal statistically significant differences, with a confidence level of 95%, particularly when PPM defoliation change exceeds 10% compared to trees with no change in defoliation (Table 4). For both crown delineation methods, in tree crowns with no change in defoliation, there is an increase in both leaf area index and mean leaf area density matching with the increase in primary production measured through normalized difference vegetation index [51], with absolute values of 0.70 and 0.07, respectively. Conversely, these LiDAR metrics exhibit significant decreases in tree crowns with a defoliation change exceeding 10%, registering reductions of up to −0.67 and −0.05 in absolute values, respectively (Figure 4, Figure A2 of Appendix A).

Table 4. Summary of the LiDAR metrics with statistically significant differences between changes in defoliation (two or three defined classes) along the PPM feeding period.

Classes of Infestation Change	LiDAR Metric	Manual Delineation ANOVA (*p* Value)	LiDAR Delineation ANOVA (*p* Value)	Transformation
2 classes (no change vs. change)	Leaf area index	0.03	0.03	None
	Mean leaf area density	0.03	0.02	None
3 (no change, small change, great change)	D9	0.05	Not significant	None
	% returns in lower 10% of maximum elevation (W1)	0.02	0.03	Logarithmic

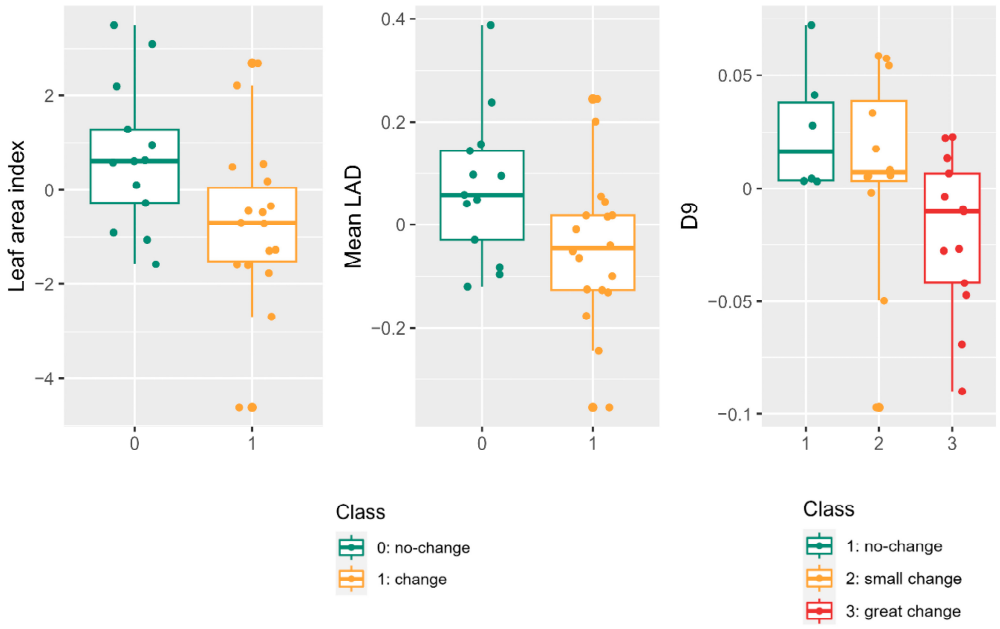

Figure 4. Boxplots of LiDAR metrics for two classes: no change vs. change in defoliation trees (class 0 vs. class 1), and three classes: no change, small change, and great change in defoliation (class 1, 2, and 3). LiDAR metrics were extracted based on manual crown delineation. LAI refers to leaf area index; Mean LAD stands for mean leaf area density; D9 is the percentage of the 9th vertical layers derived by dividing the height between the 95th percentile of the height distribution and the 2 m threshold.

Statistically significant differences were observed in two LiDAR-derived metrics across three classes of defoliation change defined using k-means (i.e., no change, small change, and great change in defoliation) during the feeding period (Table 4). The D9 metric, associated with the percentage of points in the upper vertical layer, demonstrated an average increase of 3% when no change in defoliation was detected, remaining relatively stable in the presence of a small change in defoliation. However, D9 exhibited an average decrease of 2% when substantial changes in defoliation occurred (Figure 4, Figure A2 of Appendix A). Moreover, the percentage of returns in the lower 10% of the maximum elevation exhibited an increase with defoliation, showcasing a change of 3.5% between no change and great change in defoliation classes. However, the pattern appeared less distinct for the small change class, demonstrating values similar to the no change class with a marginal difference of 0.3%.

3.3. Similarity between Manual and Automatized Tree Derived Crown Metrics for PPM Monitoring

The impact of crown delineation methodology on subsequent LiDAR metric extraction and PPM monitoring is outlined in Table 5. ANOVA comparison of extracted values between manual and LiDAR-based crown delineation did not reveal significant differences for any of the LiDAR-derived metrics identified in previous analyses (i.e., differences between non-defoliated and defoliated trees; structural changes over the PPM period of feeding) using ANOVA. As illustrated in Figure 5, an example of manual and LiDAR-based delineation is presented for the leaf area index metric. Although the absolute values of LiDAR metrics may not be identical for both delineations, minimal differences are observed, averaging 0.53 (4.26%) for the leaf area index and 0.05 (5.24%) for mean leaf area density.

Table 5. Comparison of LiDAR-derived metrics for manual and LiDAR based crown delineation.

Analysis	LiDAR Metric	Manual vs. LiDAR Delineation ANOVA (*p* Value)	Manual vs. LiDAR Delineation Tukey (MSD)
Non-defoliated vs. defoliated	Leaf area index	0.48	0.06
	Mean leaf area density	0.46	0.13
	% all returns above 2 m respect to total first returns	0.14	4.14
	W1	0.51	1.13
	W2	0.46	2.32
Changes in defoliation. No change vs. change	Leaf area index	0.81	0.82
	Mean leaf area density	0.76	0.07
Changes in defoliation. No change, small, great change	D9	0.93	0.02 *
	W1	0.96	0.95

Signif. Codes: 0.01 '*'

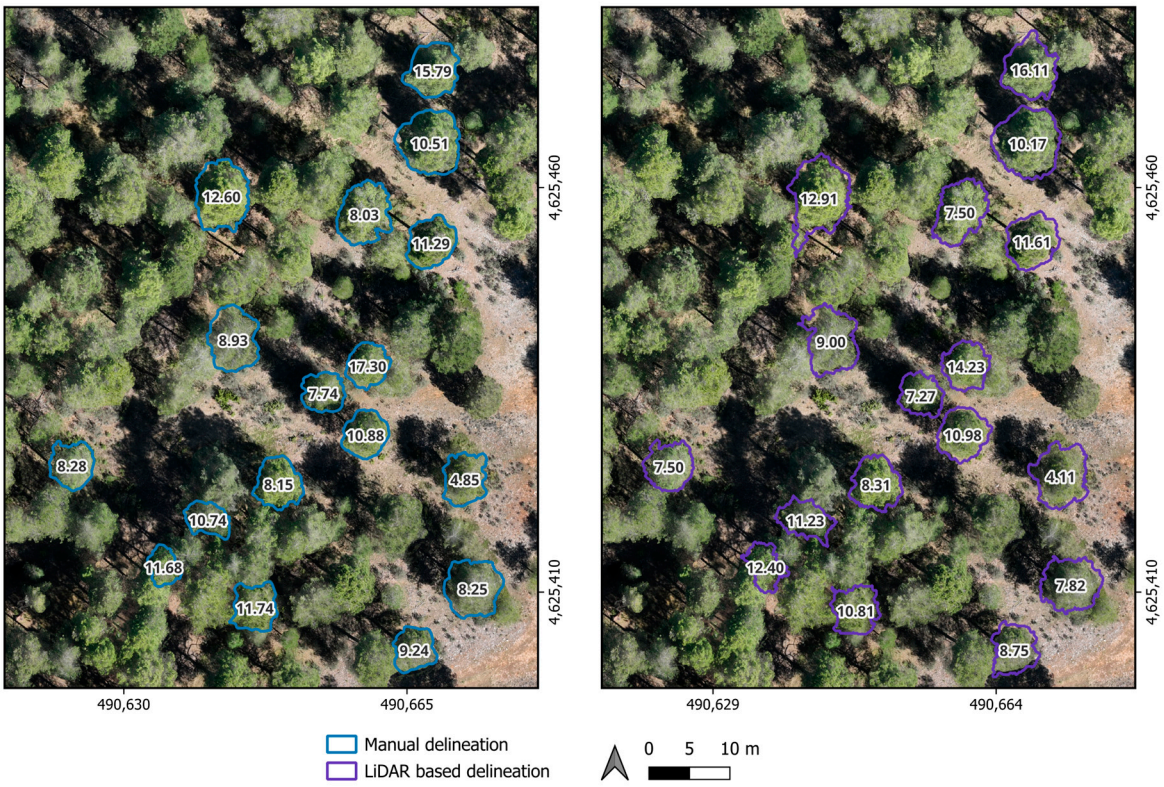

Figure 5. Comparison of leaf area index (LAI) for two delineation types: manual (**left map**) and LiDAR based (**right map**) extracted using the 24 April 2023 LiDAR flight. The numbers inside crown delineations indicate LAI derived LiDAR drone absolute values.

The post hoc Tukey test results align closely with those obtained from the ANOVA analysis. However, statistically significant differences were identified between manual and LiDAR delineation specifically in the case of the D9 metric. This outcome is consistent with the earlier analysis, where the D9 metric did not provide meaningful distinctions for determining three classes of defoliation change using the automatized crowns (see Table 4).

4. Discussion

The impact of PPM in pine forests manifests in noteworthy alterations to tree crown density. The reduction in pine needles alters plant dynamics and nutrient cycling, resulting in diminished radial tree growth and volume [52,53]. PPM-induced defoliations lead to substantial reductions in leaf area index and mean leaf area density, reaching up to 23%

when comparing non-defoliated to defoliated trees. The concurrent decrease in upper canopy density enhances LiDAR pulse penetration, yielding a notably higher percentage of returns in lower tree canopy branches. Moreover, our study unveils evident morphological transformations throughout the winter feeding period, showing statistically significant differences in two to three classes of defoliation change using drone LiDAR-derived canopy density metrics. These results hold for LiDAR-based crown delineation and provide comparable information to manual delineations. Such findings offer essential insights into the development of dynamic replicas or digital twins, facilitating enhanced forest ecosystem monitoring and informed decision-making by forest managers.

The assessment of defoliation through drone LiDAR point clouds enables the discrimination of non-defoliated and defoliated trees at the individual level. Statistically significant differences were identified for defoliation levels below or above 15%, consistent with previous assessments that employed drone multispectral images and determined a 20% defoliation threshold as optimal for recognizing defoliated trees [8]. Both LAI and mean leaf area density LiDAR metrics exhibited significant reductions in the upper canopy due to PPM infestation, aligning with findings from Solberg [54]. Solberg utilized LAI derived from high-density airborne laser scanning (ALS) data to estimate defoliations caused by *Neodiprion sertifer* and compared the results to forest cutting practices. PPM infestation prompted increased pulse penetration to lower canopy strata, resulting in significant modifications to canopy morphology resembling changes induced by low–medium–severity forest fires [55]. Interestingly, two metrics related to the cumulative proportion of returns in lower percentages of maximum elevation (W1 and W2) proved more effective than fixed height strata thresholds (e.g., returns between 3 and 4 m) in capturing the defoliation-induced changes in tree structure. The utilization of LiDAR drone technology opens new avenues for analyzing defoliations at the individual tree scale, expanding the range of available drone tools [31,32]. This underscores LiDAR's capacity to provide a three-dimensional perspective on canopy structure changes.

PPM defoliation instigates morphological transformations throughout the winter, distinctly discernible through multitemporal LiDAR drone-derived metrics. LAI and mean leaf area density exhibited significant differences, particularly in determining defoliation changes exceeding 10%, a common threshold applied in field measurements. The percentage of returns in the upper canopy layer (D9) proved valuable in detecting up to three levels of defoliation change, although caution is warranted due to potential ambiguities between no-change and small-change detections [8]. Prior research has often relied on multitemporal datasets from middle-resolution (e.g., Landsat) and low spatial resolution (e.g., MODIS) multispectral sensors for monitoring PPM outbreaks. Spectral changes observed throughout the PPM cycle enable the detection and characterization of infestation levels [28–30], typically categorizing them into two to three levels, mirroring those determined with drone LiDAR. While three-dimensional datasets are progressively becoming available, those derived from ALS remain relatively scarce [41]. Drone LiDAR has opened new opportunities for tailored multitemporal flights, augmenting spatiotemporal monitoring frequencies and facilitating fine change detections of PPM defoliations, akin to field measurements (i.e., 10% change).

Automated tree-crown delineation from 3D drone LiDAR-derived point clouds yields comparable information to manual delineation in monitoring PPM defoliation. Though our focus does not center on identifying the optimal automatic crown delineation algorithm, we have observed that commonly employed methods such as tree top [39] and tree crown watershed segmentation [40], deliver accurate LiDAR derived metrics. LAI, the mean leaf area density, the percentage of all returns above 2 m concerning the total first returns, and metrics W1 and W2 exhibit no significant differences compared to manual delineations. However, there are notable distinctions in the upper canopy layer density (D9) metric between manual and automatic delineations, necessitating further investigation across more representative spatial scales. Despite additional examinations using alternative automatic delineation methodologies and encompassing a broader range of forest stand

densities are warranted, automatic LiDAR delineation appears promising for monitoring PPM defoliation outbreaks over larger areas.

The present study underscores the utility of LiDAR drone data in delineating morphological changes in tree crowns resulting from PPM defoliations within a Mediterranean forest environment dominated by *Pinus nigra*, a highly PPM palatable species. Periodic in situ defoliation sampling at tree level and the capturing of multitemporal LiDAR flights are costly and labor intensive. This study shows that LiDAR metrics are sensitive to changes in crown morphology caused by PPM defoliations. The sample size of our study may have potentially overlooked further LiDAR metrics sensitive to PPM-induced changes in crown morphology. Despite this sample size, those LiDAR metrics that showed statistical differences in ANOVA analyses and fulfilled the normality and equal variance hypothesis, also showed significant differences in non-parametric tests (no shown), which indicates that these variables are in fact sensitive to PPM defoliations. Future research should also focus on the monitoring of wider areas (in situ and with remote sensing data) to develop statistical models to further scale the results to larger areas. Such analysis cannot be undertaken with the present dataset due to limitations in our sample size. However, our results provide useful insights for modeling efforts in larger areas, presenting a set of LiDAR metrics to prioritize when developing predictive models. As high-density 3D LiDAR drone point clouds continue to represent a novel source of information, future research endeavors should prioritize their integration with multispectral drone-derived datasets, high-resolution satellite imagery or intensity-derived LiDAR metrics to characterize PPM defoliations at broader scales. Our study quasi covers a major feeding period in winter, but some specific trees presented defoliation levels during the end of December, and further research should focus on the complete PPM cycle period. Considering the effectiveness of specific LiDAR metrics for PPM monitoring, the utilization of photogrammetric point clouds may prove advantageous due to the increased affordability of RGB or multispectral sensors. Overall, future endeavors should focus on multi-scale and multi-sensor approaches, from in situ measurements up to satellite datasets, to enable near-real time monitoring and early warming detection for better forest management.

5. Conclusions

This study highlights the efficacy of high-density drone LiDAR 3D point clouds in elucidating the impact of PPM on the canopy morphology of Mediterranean *Pinus nigra* forests. Our findings underscore a significant reduction in both leaf area index and mean leaf area density, reaching up to 23% compared to healthy tree crowns. Defoliations occurring in the upper canopy layers increase pulse penetration, resulting in a significantly higher percentage of returns in lower tree canopy layers and inducing modifications to tree crown shape. Drone LiDAR datasets facilitate defoliation monitoring throughout the winter feeding period, discriminating changes in defoliation levels of up to 10%, aligning with visually acquired field measurements. Furthermore, our results suggest the practicality of automatic tree-crown LiDAR-based delineation for defoliation monitoring over larger areas. Overall, this study represents an initial exploration into the utility of high-density drone LiDAR data for ad hoc monitoring of PPM defoliations, providing valuable support for forest management initiatives.

Author Contributions: Conceptualization, D.D., C.G. and F.R.-P.; methodology, D.D., C.G., F.M. and F.R.-P.; formal analysis, D.D. and F.R.-P.; resources, D.D., C.G., F.M., H.H., G.S.-B. and F.R.-P.; data curation, D.D., F.M., H.H. and F.R.-P.; writing—original draft preparation, D.D.; writing—review and editing, C.G., F.M., H.H., G.S.-B. and F.R.-P.; funding acquisition, G.S.-B. All authors have read and agreed to the published version of the manuscript.

Funding: This research was funded by projects: PROWARM (PID2020-118444GA-I00) from the MCIN/AEI/10.13039/501100011033, OUTBREAK (VA171P20) from Junta de Castilla y León Government, and CLU-2019-01–iuFOR Institute Unit of Excellence of the University of Valladolid from Junta de Castilla y León and co-financed by the European Union (ERDF "Europe drives our growth"). D. Domingo acknowledges support by the European Union-NextGeneration EU Margarita Salas

(MS-240621). Francisco Mauro was supported by the Maria Zambrano's Excellence Program (#E-42-2022-0000233) from the Ministry of Science and Innovation and funded by the University of Valladolid and European Union-NextGeneration EU. Hermine Houdas was supported by a predoctoral contract (PRE2021-098278), funded by MCIN/AEI/10.13039/501100011033 and ESF "Investing in your future". G. Sangüesa-Barreda was supported by a Postdoctoral grant (IJC2019-040571-I) funded by MCIN/AEI/10.13039/501100011033.

Data Availability Statement: The data presented in this study are available upon request from the corresponding author.

Acknowledgments: We are grateful to Héctor Hernández-Alonso who helped in the field data collection.

Conflicts of Interest: The authors declare no conflicts of interest.

Appendix A

Table A1. Summary Mavic 3 Multispectral (M3M) 24-04-2023 flight used for manual tree crown delineation.

Characteristics	Acquisition
Date (day-month-year)	24 April 2023
Side Overlap (%)	80
Front Overlap (%)	80
Flight Height (m)	90
RGB Resolution (cm)	2.89
Number of Images	155
Flight Time (min)	8.28
Area (ha)	11.80

Table A2. Summary of the drone LiDAR computed metrics, including the abbreviations, classes, and macro-classes defined.

Macro-Classes	Classes	ALS Computed Metrics	Abbreviations
Canopy height metrics (CHM)	Lower height variables	Minimum elevation	Elev. minimum
		01th percentile of the return heights	P01
		05th percentile of the return heights	P05
		10th percentile of the return heights	P10
		20th percentile of the return heights	P20
		25th percentile of the return heights	P25
		L moment 1 elevation	Elev. L1
		L moment 2 elevation	Elev. L2
	Mean height variables	Mean elevation	Elev. Mean
		Mode elevation	Elev. Mode
		30th percentile of the return heights	P30
		40th percentile of the return heights	P40
		50th percentile of the return heights	P50
		60th percentile of the return heights	P60
		70th percentile of the return heights	P70
		L moment 3 elevation	Elev. L3
		Elevation quadratic mean	Elev. SQRT mean SQ
		Elevation cubic mean	Elev. CUR mean CUBE
	Higher height variables	75th percentile of the return heights	P75
		80th percentile of the return heights	P80
		90th percentile of the return heights	P90
		95th percentile of the return heights	P95
		99th percentile of the return heights	P99
		Maximum elevation	Elev. maximum
		L moment 4 elevation	Elev. L4

Table A2. *Cont.*

Macro-Classes	Classes	ALS Computed Metrics	Abbreviations
Canopy height variability metrics (CHVM)	Variability	Standard deviation of point heights distribution	Elev. SD
		Variance of point heights distribution	Elev. Variance
		Coefficient of variation of point heights distribution	Elev. CV
		Skewness of point heights distribution	Elev. Skewness
		kurtosis of point heights distribution	Elev. Kurtosis
		Interquartile distance of point heights distribution	Elev. IQ
		Average Absolute Deviation of point heights distribution	Elev. AAD
		Mean absolute deviation from the mean	Desviation.mean
		Mean absolute deviation from the median	Desviation.median
	Variability L moment	L moment coefficient of variation of point heights distribution	Elev. LCV
		L moment skewness of point heights distribution	Elev. Lskewness
		L moment kurtosis of point heights distribution	Elev. Lkurtosis
Canopy density metrics (CDM)	% first, % all returns, % by height thresholds, % equally vertical layers, gap space, leaf area, canopy relief ratio	percentage of first returns above 2.00	% first ret. above 2.00
		percentage of all returns above 2.00	% all ret. above 2.00
		percentage of first returns above the mean	% first ret. above mean
		percentage of first returns above the mode	% first ret. above mode
		percentage of all returns above the mean	% all ret. above mean
		percentage of all returns above the mode	% all ret. above mode
		percentage of all returns every 1m (between 2 and 30 m)	e.g., % all ret. 10 to 11
		Percentage of all returns in 10 equally distributed vertical layers derived by dividing the height between the 95th percentile of the height distribution and the 2 m threshold	D0, D1, : : : ,D9
		Canopy density metrics as defined by Woods et al. [48] % returns in 10 equally distributed layers respect to maximum elevation	W1, W2, : : : ,W9
		Open gap space	Open gap space
		Closed gap space	Closed gap space
		Euphotic	Euphotic
		Oligophotic	Oligophotic
		Leaf area index	LAI
		Mean leaf area density	Mean leaf area density
		Maximum leaf area density	Max. leaf area density
		Minimum leaf area density	Min. leaf area density
		Coefficient of variation leaf area density	CV. leaf area density
		Canopy relief ratio	CRR
	All returns Total returns-1	All returns above 2.00 divided by the total first returns × 100	(All ret. above 2.00)/(total first ret.) × 100
		All returns above mean divided by the total first returns × 100	(All ret. above mean)/(total first ret.) × 100
		All returns above mode divided by the total first returns × 100	(All ret. above mode)/(total first ret.) × 100
Structural diversity indices (SDI)		Shannon diversity index	Shannon
		Vertical complexity index	VC
		Rumple index	Rumple
Voxel metrics		Total number of filled voxels	V.n
		Standard deviation of voxel elevation	V.sd
		Coefficient of variation of voxel elevation	V.cv
		Ratio between filled voxels and total number of voxels	V. ratio filled
		Vertical rumple based on voxels	V. rumple

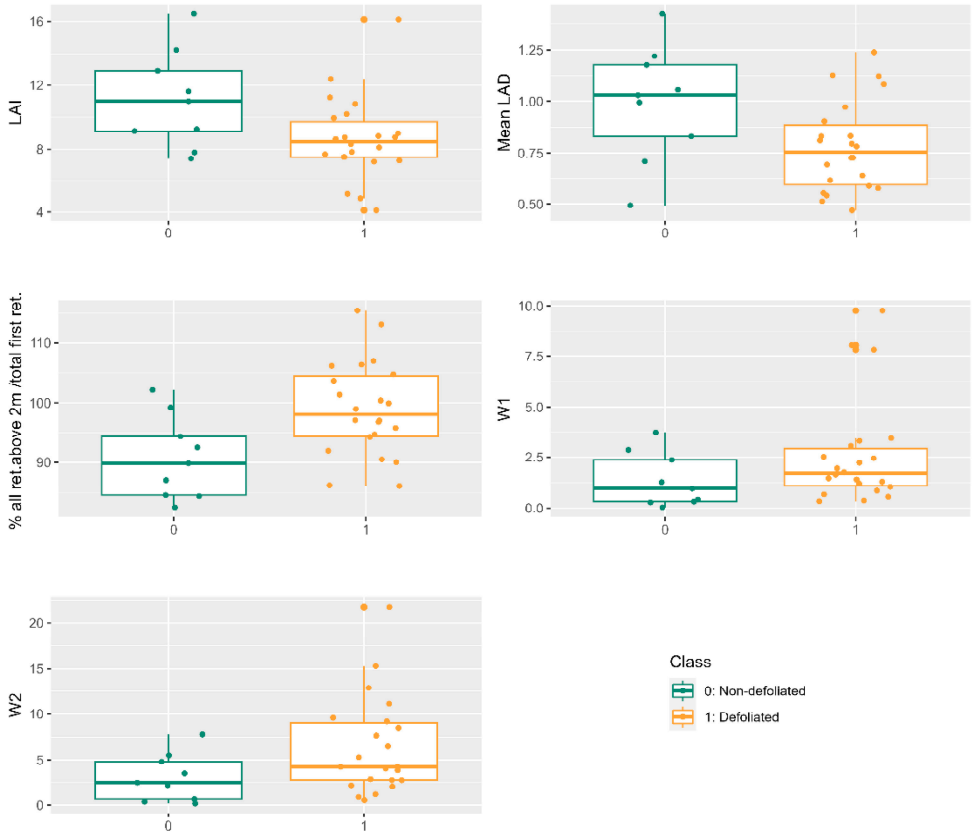

Figure A1. Boxplots of LiDAR metrics for non-defoliated vs. defoliated trees (class 0 vs. class 1) for LiDAR based crown delineation. LAI refers to leaf area index; Mean LAD stands for mean leaf area density; % all ret. above 2 m/total first ret. refers to the percentage of all returns above 2 m respect to total first returns; W1 and W2 are the % returns in lower 10 or 20% of maximum elevation, respectively.

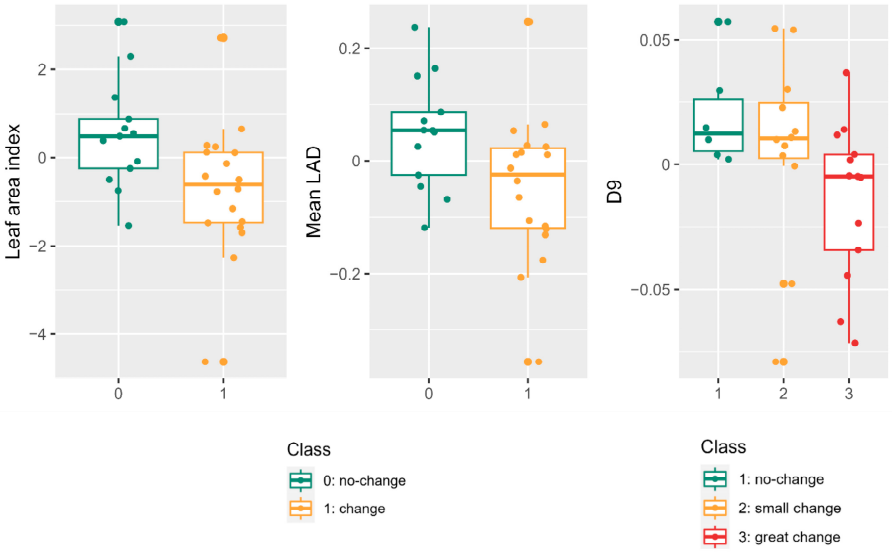

Figure A2. Boxplots of LiDAR metrics for two classes: no change vs. change in defoliation trees (class 0 vs. class 1), and three classes: no change, small change, and great change in defoliation (class 1, 2, 3). LiDAR metrics were extracted based on LiDAR based crown delineation. LAI refers to leaf area index; Mean LAD stands for mean leaf area density; D9 is the percentage of the 9th vertical layers derived by dividing the height between the 95th percentile of the height distribution and the 2 m threshold.

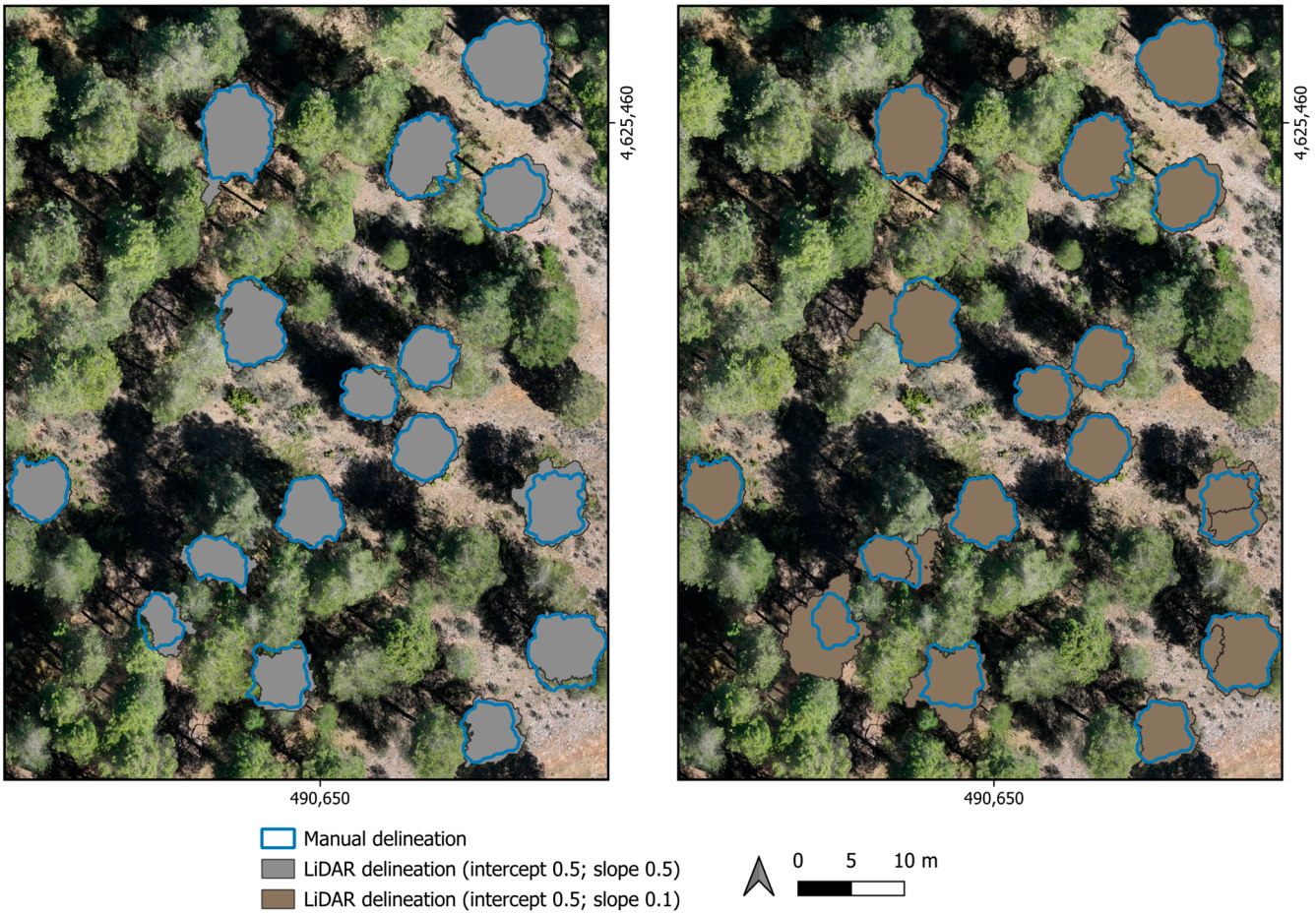

Figure A3. Comparison of manual crown delineation respect to two selected parametrizations of LiDAR based crown delineation. Intercept 0.5 and slope 0.5 (**left**); intercept 0.5 and slope 0.1 (**right**). Delineations are carried out based on 24 April 2023 flight.

References

1. Millar, C.I.; Stephenson, N.L. Temperate forest health in an era of emerging megadisturbance. *Science* **2015**, *349*, 823–826. [CrossRef] [PubMed]
2. Hamann, E.; Blevins, C.; Franks, S.J.; Jameel, M.I.; Anderson, J.T. Climate change alters plant–herbivore interactions. *New Phytol.* **2021**, *229*, 1894–1910. [CrossRef] [PubMed]
3. Seidl, R.; Schelhaas, M.J.; Rammer, W.; Verkerk, P.J. Increasing forest disturbances in Europe and their impact on carbon storage. *Nat. Clim. Chang.* **2014**, *4*, 806–810. [CrossRef] [PubMed]
4. Jacquet, J.S.; Orazio, C.; Jactel, H. Defoliation by processionary moth significantly reduces tree growth: A quantitative review. *Ann. For. Sci.* **2012**, *69*, 857–866. [CrossRef]
5. Seidl, R.; Rammer, W. Climate change amplifies the interactions between wind and bark beetle disturbances in forest landscapes. *Landsc. Ecol.* **2017**, *32*, 1485–1498. [CrossRef] [PubMed]
6. Roques, A. *Processionary Moths and Climate Change: An Update*; Springer: Berlin/Heidelberg, Germany, 2015; ISBN 9789401793407.
7. Montoya Moreno, R.; Hernández Alonso, R.; Pérez Fortea, V.; Martín Bernal, E. *Procesionaria del Pino*; Servicio de Estudios, Coordinación y Defensa Contra Incendios Forestales; Gobierno de Aragon: Zaragoza, Spain, 2022.
8. Cardil, A.; Vepakomma, U.; Brotons, L. Assessing Pine Processionary Moth Defoliation Using Unmanned Aerial Systems. *Forests* **2017**, *8*, 402. [CrossRef]
9. Battisti, A. Host-plant relationships and population dynamics of the Pine Processionary Caterpillar *Thaumetopoea pityocampa* (Denis & Schiffermuller). *J. Appl. Entomol.* **1988**, *105*, 393–402. [CrossRef]
10. Hódar, J.A.; Castro, J.; Zamora, R. Pine processionary caterpillar *Thaumetopoea pityocampa* as a new threat for relict Mediterranean Scots pine forests under climatic warming. *Biol. Conserv.* **2003**, *110*, 123–129. [CrossRef]
11. Moneo, I.; Battisti, A.; Dufour, B.; García-Ortiz, J.C.; González-Muñoz, M.; Moutou, F.; Paolucci, P.; Petrucco Toffolo, E.; Rivière, J.; Rodríguez-Mahillo, A.I.; et al. Medical and veterinary impact of the urticating processionary larvae. In *Processionary Moths and Climate Change: An Update*; Springer: Dordrecht, The Netherlands, 2015; pp. 359–410.

12. Régolini, M.; Castagneyrol, B.; Dulaurent-Mercadal, A.M.; Piou, D.; Samalens, J.C.; Jactel, H. Effect of host tree density and apparency on the probability of attack by the pine processionary moth. *For. Ecol. Manag.* **2014**, *334*, 185–192. [CrossRef]
13. Azcárate, F.M.; Seoane, J.; Silvestre, M. Factors affecting pine processionary moth (*Thaumetopoea pityocampa*) incidence in Mediterranean pine stands: A multiscale approach. *For. Ecol. Manag.* **2023**, *529*, 120728. [CrossRef]
14. Huchon, H.; Demolin, G. La bioécologie de la Processionnaire du pin: Dispersion potentielle, dispersion actuelle. *Rev. For. Française* **1970**, *22*, 220–234. [CrossRef]
15. Battisti, A.; Stastny, M.; Netherer, S.; Robinet, C.; Schopf, A.; Roques, A.; Larsson, S. Expansion of geographic range in the pine processionary moth caused by increased winter temperatures. *Ecol. Appl.* **2005**, *15*, 2084–2096. [CrossRef]
16. Robinet, C.; Rousselet, J.; Roques, A. Potential spread of the pine processionary moth in France: Preliminary results from a simulation model and future challenges. *Ann. For. Sci.* **2014**, *71*, 149–160. [CrossRef]
17. Rocha, S.; Kerdelhué, C.; Ben Jamaa, M.L.; Dhahri, S.; Burban, C.; Branco, M. Effect of heat waves on embryo mortality in the pine processionary moth. *Bull. Entomol. Res.* **2017**, *107*, 583–591. [CrossRef] [PubMed]
18. Bourougaaoui, A.; Ben Jamâa, M.L.; Robinet, C. Has North Africa turned too warm for a Mediterranean forest pest because of climate change? *Clim. Chang.* **2021**, *165*, 46. [CrossRef]
19. Robinet, C.; Rousselet, J.; Pineau, P.; Miard, F.; Roques, A. Are heat waves susceptible to mitigate the expansion of a species progressing with global warming? *Ecol. Evol.* **2013**, *3*, 2947–2957. [CrossRef]
20. Domingo, D.; Vicente-serrano, S.M.; Cristina, G.; Sangüesa-barreda, G. Summer heat waves could counterbalance the increasing incidence of pine processionary due to warmer winters in Mediterranean pine forests. *For. Ecol. Manag.* **2024**, *555*, 121695. [CrossRef]
21. Rocha, S.; Caldeira, M.C.; Burban, C.; Kerdelhué, C.; Branco, M. Shifted phenology in the pine processionary moth affects the outcome of tree-insect interaction. *Bull. Entomol. Res.* **2020**, *110*, 68–76. [CrossRef]
22. Hódar, J.A.; Zamora, R.; Castro, J. Host utilisation by moth and larval survival of pine processionary caterpillar *Thaumetopoea pityocampa* in relation to food quality in three Pinus species. *Ecol. Entomol.* **2002**, *27*, 292–301. [CrossRef]
23. Samalens, J.C.; Rossi, J.P. Does landscape composition alter the spatiotemporal distribution of the pine processionary moth in a pine plantation forest? *Popul. Ecol.* **2011**, *53*, 287–296. [CrossRef]
24. Castagneyrol, B.; Régolini, M.; Jactel, H. Tree species composition rather than diversity triggers associational resistance to the pine processionary moth. *Basic Appl. Ecol.* **2014**, *15*, 516–523. [CrossRef]
25. Castagneyrol, B.; Kozlov, M.V.; Poeydebat, C.; Toïgo, M.; Jactel, H. Associational resistance to a pest insect fades with time. *J. Pest Sci.* **2020**, *93*, 427–437. [CrossRef]
26. Montoya Moreno, R. La procesionaria del pino. In *Plagas de Insectos en las Masas Forestales Españolas*; Ministerio de Agricultura, Pesca y Alimentación: Madrid, Spain, 1998; pp. 67–84.
27. Senf, C.; Seidl, R.; Hostert, P. Remote sensing of forest insect disturbances: Current state and future directions. *Int. J. Appl. Earth Obs. Geoinf.* **2017**, *60*, 49–60. [CrossRef]
28. Bories, N.; Samalens, J.C.; Guyon, D.; Breda, N.; Wigneron, J.P. Monitoring pine defoliation due to the processionary moth at regional scale from MODIS time series. In Proceedings of the 2012 IEEE International Geoscience and Remote Sensing Symposium, Munich, Germany, 22–27 July 2012; pp. 3383–3386. [CrossRef]
29. Sangüesa-Barreda, G.; Camarero, J.J.; García-Martín, A.; Hernández, R.; de la Riva, J. Remote-sensing and tree-ring based characterization of forest defoliation and growth loss due to the Mediterranean pine processionary moth. *For. Ecol. Manag.* **2014**, *320*, 171–181. [CrossRef]
30. Pérez-Romero, J.; Navarro-Cerrillo, R.M.; Palacios-Rodriguez, G.; Acosta, C.; Mesas-Carrascosa, F.J. Improvement of Remote Sensing-Based Assessment of Defoliation of *Pinus* spp. Caused by *Thaumetopoea pityocampa* Denis and Schiffermüller and Related Environmental Drivers in Southeastern Spain. *Remote Sens.* **2019**, *11*, 1736. [CrossRef]
31. Cardil, A. Quantifying pine processionary moth defoliation in a pine-oak mixed forest using unmanned aerial systems and multispectral imagery (dataset, paper published in *PLoS ONE*). *PLoS ONE* **2019**, *14*, e0213027. [CrossRef]
32. Otsu, K.; Pla, M.; Duane, A.; Cardil, A.; Brotons, L. Estimating the Threshold of Detection on Tree Crown Defoliation Using Vegetation Indices from UAS Multispectral Imagery. *Drones* **2019**, *3*, 80. [CrossRef]
33. Otsu, K.; Pla, M.; Vayreda, J.; Brotons, L. Calibrating the Severity of Forest Defoliation by Pine Processionary Moth with Landsat and UAV Imagery. *Sensors* **2018**, *18*, 3278. [CrossRef]
34. Garcia, A.; Samalens, J.C.; Grillet, A.; Soares, P.; Branco, M.; van Halder, I.; Jactel, H.; Battisti, A. Testing early detection of pine processionary moth *Thaumetopoea pityocampa* nests using UAV-based methods. *NeoBiota* **2023**, *84*, 267–279. [CrossRef]
35. Axelsson, P. DEM Generation from Laser Scanner Data Using Adaptive TIN Models. *ISPRS-Int. Arch. Photogramm. Remote Sens. Spat. Inf. Sci.* **2000**, *33*, 110–117.
36. Isenburg, M. LAStools-Efficient LiDAR Processing Software, Version 141017, Academic 2017. Available online: http://rapidlasso.com/LAStools (accessed on 3 January 2024).
37. McGaughey, R.J. *FUSION/LDV: Software for LIDAR Data Analysis and Visualization*, March 2014—FUSION, version 3.42; United States Department Agriculture Forest Service Pacific Northwest Research Station: Seattle, WA, USA, 2014.
38. Andrew Plowright ForestTools: Tools for Analyzing Remote Sensing Forest Data. R Package Version 1.0.0. Available online: https://github.com/andrew-plowright/ForestTools (accessed on 3 January 2024).

39. Popescu, S.C.; Wynne, R.H. Seeing the trees in the forest: Using lidar and multispectral data fusion with local filtering and variable window size for estimating tree height. *Photogramm. Eng. Remote Sens.* **2004**, *70*, 589–604. [CrossRef]
40. Meyer, F.; Beucher, S. Morphological segmentation. *J. Vis. Commun. Image Represent* **1990**, *1*, 21–46. [CrossRef]
41. Domingo, D.; Alonso, R.; Lamelas, M.T.; Montealegre, A.L.; Rodríguez, F.; de la Riva, J. Temporal transferability of pine forest attributes modeling using low-density airborne laser scanning data. *Remote Sens.* **2019**, *11*, 261. [CrossRef]
42. Næsset, E. Practical large-scale forest stand inventory using a small-footprint airborne scanning laser. *Scand. J. For. Res.* **2004**, *19*, 164–179. [CrossRef]
43. Tompalski, P.; Roussel, J.; Woods, M.; Hambrecht, L. Available online: https://github.com/ptompalski/lidRmetrics (accessed on 3 January 2024).
44. van Ewijk, K.Y.; Treitz, P.M.; Scott, N.A. Characterizing forest succession in central Ontario using lidar-derived indices. *Photogramm. Eng. Remote Sens.* **2011**, *77*, 261–269. [CrossRef]
45. Kane, V.R.; Bakker, J.D.; McGaughey, R.J.; Lutz, J.A.; Gersonde, R.F.; Franklin, J.F. Examining conifer canopy structural complexity across forest ages and elevations with LiDAR data. *Can. J. For. Res.* **2010**, *40*, 774–787. [CrossRef]
46. Nilsson, M. Estimation of tree heights and stand volume using an airborne lidar system. *Remote Sens. Environ.* **1996**, *56*, 1–7. [CrossRef]
47. Næsset, E.; Økland, T. Estimating tree height and tree crown properties using airborne scanning laser in a boreal nature reserve. *Remote Sens. Environ.* **2002**, *79*, 105–115. [CrossRef]
48. Woods, M.; Lim, K.; Treitz, P. Predicting forest stand variables from LiDAR data in the Great Lakes—St. Lawrence forest of Ontario. *For. Chron.* **2011**, *84*, 827–839. [CrossRef]
49. Lefsky, M.A.; Cohen, W.B.; Acker, S.A.; Parker, G.G.; Spies, T.A.; Harding, D. Lidar Remote Sensing of the Canopy Structure and Biophysical Properties of Douglas-Fir Western Hemlock Forests. *Remote Sens. Environ.* **1999**, *70*, 339–361. [CrossRef]
50. de Almeida, D.R.A.; Stark, S.C.; Shao, G.; Schietti, J.; Nelson, B.W.; Silva, C.A.; Gorgens, E.B.; Valbuena, R.; de Papa, D.A.; Brancalion, P.H.S. Optimizing the Remote Detection of Tropical Rainforest Structure with Airborne Lidar: Leaf Area Profile Sensitivity to Pulse Density and Spatial Sampling. *Remote Sens.* **2019**, *11*, 92. [CrossRef]
51. Aragones, D.; Rodriguez-Galiano, V.F.; Caparros-Santiago, J.A.; Navarro-Cerrillo, R.M. Could land surface phenology be used to discriminate Mediterranean pine species? *Int. J. Appl. Earth Obs. Geoinf.* **2019**, *78*, 281–294. [CrossRef]
52. Carus, S. Effects of defoliation caused by the processionary moth on growth of Crimean pines in western Turkey. *Phytoparasitica* **2009**, *37*, 105–114. [CrossRef]
53. Kurz, W.A.; Dymond, C.C.; Stinson, G.; Rampley, G.J.; Neilson, E.T.; Carroll, A.L.; Ebata, T.; Safranyik, L. Mountain pine beetle and forest carbon feedback to climate change. *Nature* **2008**, *452*, 987–990. [CrossRef]
54. Solberg, S. Mapping gap fraction, LAI and defoliation using various ALS penetration variables. *Int. J. Remote Sens.* **2010**, *31*, 1227–1244. [CrossRef]
55. Montealegre, A.; Lamelas, M.; Tanase, M.; de la Riva, J. Forest Fire Severity Assessment Using ALS Data in a Mediterranean Environment. *Remote Sens.* **2014**, *6*, 4240–4265. [CrossRef]